RSC Advances

PAPER

View Article Online
View Journal | View Issue

Cite this: *RSC Adv.*, 2020, **10**, 14979

Efficient removal of Cu(II) from aqueous systems using enhanced quantum yield nitrogen-doped carbon nanodots†

Mohammed Abdullah Issa, * Zurina Z. Abidin, * Musa Y. Pudza and Hamid Zentou

The valorization of cellulose-based waste is of prime significance to green chemistry. However, the full exploitation of these lignocellulosic compounds to produce highly luminescent nanoparticles under mild conditions has not yet been achieved. In this context, we convert low-quality waste into value-added nanomaterials for the removal of Cu(II) from wastewater. Carboxymethylcellulose (CMC), which was derived from empty fruit bunches, was selected for its high polymerization index to produce luminescent nitrogen-doped carbon dots (N-CDs) with the assistance of polyethylene glycol (PEG) as a dopant. The optimum N-CD sample with the highest quantum yield (QY) was characterized using various analytical techniques and the results show that the N-CDs have great crystallinity, are enriched with active sites and exhibit a long-shelf life with an enhanced QY of up to 27%. The influence of Cu^{2+} concentration, adsorbent (N-CDs) dosage, pH and contact time were investigated for the optimal adsorption of Cu^{2+}. The experiments showed the rapid adsorption of Cu^{2+} within 30 min with a removal efficiency of over 83% under optimal conditions. The equilibrium isotherm investigation revealed that the fitness of the Langmuir isotherm model and kinetic data could be well explained by the pseudo-second order model. Desorption experiments proved that N-CDs can be regenerated successfully over five adsorption–desorption cycles owing to the ability of ascorbic acid (AA) to reduce the adsorbed nanocomplex into Cu^{+}. The rapid adsorption property using low-cost materials identifies N-CDs as a superior candidate for water remedy.

Received 11th March 2020
Accepted 31st March 2020

DOI: 10.1039/d0ra02276d

rsc.li/rsc-advances

1. Introduction

Water pollution caused by toxic Cu(II) metal has become a worldwide issue owing to its severe threat to human health and the environment.[1,2] Toxic Cu(II) can easily enter the food chain *via* anthropogenic activities causing diverse diseases in humans.[3] Cu(II) is widely found in the environment, industries, and domestic functions. The excessive intake of copper has detrimental impacts on human health that include disorders of the nervous, immune, reproductive and gastrointestinal systems.[4,5] Based on the World Health Organization and Environmental Protection Agency, the permissible limits of Cu(II) in drinking water is 2 and 1.3 mg L^{-1}, respectively.[5] Thus, the separation and elimination of Cu(II) from the aquatic environment is still a hot topic due to its toxic effect on human health.

Many protocols have been reported for Cu(II) removal from water like reverse osmosis, ion-exchange, electrochemical removal and adsorption.[2,6] Among the above protocols, adsorption is the most used for its simplicity, low-toxicity and ease of operation. Recently, the usage of fluorescent nanomaterials has been well-documented in the recognition of contaminates using fluorescence quenching and electrochemical removal, which typically occurs *via* an adsorption mechanism.[7–11] Despite their ability to enhance the sensing performance, several drawbacks of using these nanomaterials, such as high toxicity and complex operational steps, limit their practical applications. For instance, high sensitivity was obtained using semiconductor quantum dots (QDs), but the introduction of intrinsically toxic elements affects their performance as ideal systems.[9,12,13] Additionally, the fabrication of metal-based nanomaterials such as Au and Ag with electrochemical techniques requires extensive pre-treatments of the electrode surface, like polishing and surface contamination oxidation among others, restricting their practical applications. Recently, carbon dots (CDs) have been exploited for novel applications due to their impressive optical features. However, the encapsulation of CDs into solid-state films is still challenging as they exhibit self-quenching phenomena after the immobilization processes, making them unsuitable for application in a variety of fields.

Contrary to QDs, carbon dots (CDs) are composed of intrinsically non-toxic carbon.[14] CDs consist of a graphitic or

Department of Chemical and Environmental Engineering, Faculty of Engineering, Universiti Putra Malaysia, 43400 UPM Serdang, Selangor, Malaysia. E-mail: mohbaghdadi1@yahoo.com; zurina@upm.edu.my

† Electronic supplementary information (ESI) available. See DOI: 10.1039/d0ra02276d

amorphous carbon core coated with oxygen-functionalities, polymers and other active groups based on the synthesis conditions and surface chemistry.[15] The novel properties in terms of biocompatibility and photoluminescence in addition to the large diversity of carbonaceous precursors make CDs ideal in the fields of wastewater treatment, photocatalysis, bioimaging, cancer therapy and chemical sensing.[16–20] In this regard, various carbon-rich resources have been employed as single precursors for the production of CDs.[21–23] However, the latter show weaker PL compared to those from dual precursors. Doping CDs with non-metal moieties such as N dopants has been considered as the most promising approach to QY enhancement by tuning the upward shift of the Fermi level.[18,24]

On the other hand, the usage of biomass resources, particularly lignocellulosic waste, has been recently reported for the synthesis of heteroatom-doped CDs, in which various QYs were obtained using different synthesis conditions (Table 1). It is well known that the formation of CDs is highly dependent on the substitution degree of the cellulose structure, the chain length of the cellulose backbone, the clustering degree of the cellulose substituents, as well as the choice of dopant and influence of the passivating species. Most reported works show several shortcomings including low fluorescence QY and long preparation time.[25,26] These drawbacks may relate to the absence of ether groups within the cellulose framework resulting in a lower substitution reaction. Carboxymethylcellulose (CMC) from empty fruit bunches (EFBs) is rich with ether and hydroxyl groups, which could play a major role in the successive rearrangement reactions leading to process acceleration. Thus, the full exploitation of these waste products to recycle them and develop new value-added carbon nanomaterials is of great interest.

In this work, we report the eco-friendly synthesis of N-CDs from EFB carboxymethylcellulose and PEG as the carbon and nitrogen sources, respectively. The obtained N-CDs were applied for the rapid removal of Cu(II) from contaminated water. The properties of N-CDs were established using TEM, HRTEM, XRD, FTIR, XPS, UV-vis, PL and zeta potential. The influence of the initial concentration, adsorbent dosage, pH and contact time on the removal efficiency of Cu(II) using N-CDs was studied using batch adsorption tests. The adsorption isotherms and kinetic models were demonstrated and emphasis was placed on the adsorption mechanism through studying the interaction of Cu(II) with N-CDs.

2. Experimental

2.1 Materials

CMC of oil palm empty fruit bunches (EFBs) were purchased from Waris Nove Company, Malaysia. Polyethylene glycol (M.W. 400) and quinine sulfate were obtained from Sigma-Aldrich (USA). Deionized water (DI) was used throughout all the experiments. All the chemicals used were of analytical grade and used as received without further modification.

2.2 Preparation of N-CDs

First, 0.2 g of fine CMC was mixed with 30 mL of PEG and dispersed into 25 mL of DI water by means of ultrasonication. The mixture was then transferred to a 50 mL Teflon-lined stainless-steel reactor, sealed and heated at 270 °C for 6 h in an oven. The obtained solution was cooled down at room temperature and then centrifuged at 10 000 rpm for 12 min to remove the larger size particles. To further isolate the smaller particle size of N-CDs and eliminate salt ions, purification was done with vacuum filtration (0.22 μm) and a dialysis membrane (1 kDa), respectively. For comparison, undoped CDs were prepared using a similar manner as that used for the production of N-CDs, except for the addition of PEG.

2.3 Characterization of adsorbent

Transmission electron microscopy (TEM) and high-resolution TEM (HRTEM) measurements were carried out using a Tecnai G2 F20 electron microscope, with an acceleration voltage of 200 kV. X-ray powder diffraction (XRD) patterns were measured using a PANalytical diffractometer with Cu-Kα radiation. The Fourier transform infrared (FTIR) (Thermo Nicolet FT-IR spectrometer of 4 cm^{-1} resolution) was measured with KBr as a standard within the range from 650 to 4000 cm^{-1}. X-ray photoelectron spectra (XPS) (Physical Electronics PHI 5400 spectrometer, Mimos Semiconductors, Malaysia) were collected using Al-Kα radiation ($h\nu = 1486.6$ eV). Prior to de-convolution, charge correction was established at C_{1s} by setting the binding energies of C–C and C–H at 284.8 eV. The pH values were obtained by a PB-10 pH-meter (Beijing Sartorius Instruments Co. Ltd., China) and the zeta potential study of N-CDs was carried out using a Zetasizer Nano ZS (Malvern, UK). The UV-vis spectra of all samples were recorded using Shimadzu UV-1800 spectrophotometer. Fluorescence studies were measured in quartz

Table 1 A summary of different cellulose biomasses with heteroatom-doping for the synthesis of CDs *via* a hydrothermal route

Type	Starting material	Synthetic method	QY	Ref.
CDs	CMC	210 °C, 12 h	6.2%	27
N-CDs	Cellulose, urea	180 °C, 72 h	21%	28
N-CDs	CMC, urea	210 °C, 12 h	18%	29
N-CDs	CMC, EDA	270 °C, 6 h	22.9%	30
N-CDs	Microcrystalline cellulose, EDA	240 °C, 12 h	51%	31
N/Al-CDs	Durian shell cellulose, urea, $Al(NO_3)_3$	210 °C, 12 h	28.7%	32
N-CDs	Durian shell cellulose, urea	210 °C, 12 h	10.4%	32
S-CQDs	Cellulose, sulfuric acid	200 °C, 4 h	32%	33

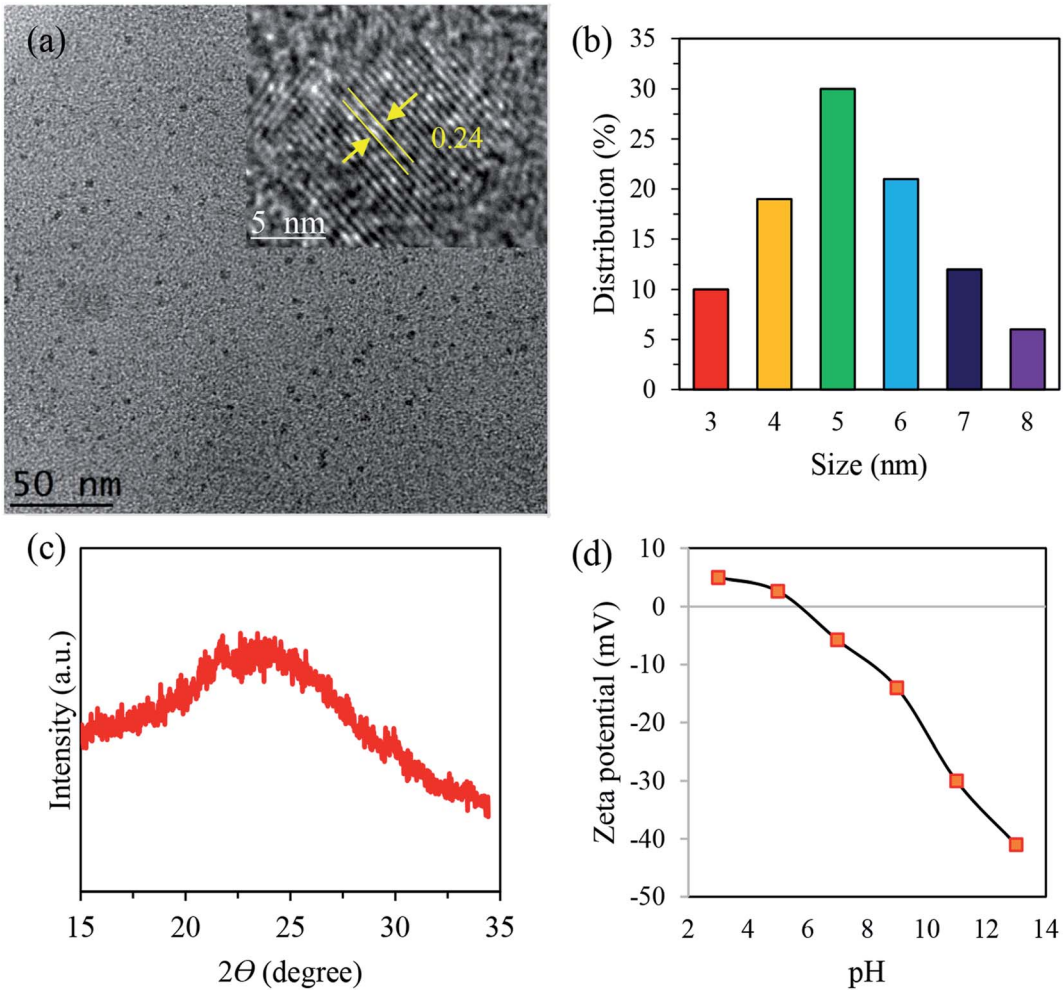

Fig. 1 (a) TEM image of N-CDs, (b) particle size distribution, (c) XRD pattern of N-CDs and (d) zeta potential study of N-CDs at different pH values. The inset shows HRTEM the image.

cuvettes with a 1 cm path length using an LS 55 Fluorescence Spectrometer (PerkinElmer, USA) with a slit width of 15 and 5 nm for excitation and emission, respectively, and a scan rate of 240 nm min^{-1}.

2.4 Quantum yield calculations

The QY of the N-CDs was calculated using quinine sulfate (QS) as a reference at a similar excitation wavelength. To guarantee a linear relationship between the absorbance and the concentration, optical densities of 0, 0.02, 0.04, 0.06, 0.08, and 0.1 were made for both the N-CD suspensions and QS at an absorption wavelength of 330 nm. Quinine sulfate (literature QY = 0.54) was dissolved in 0.1 M H_2SO_4 (refractive index (η) of 1.33) while the N-CD samples were dissolved in water ($\eta = 1.33$). Taking the optimal sample as an example, PL spectra were recorded at an excitation of 330 nm. Then, by comparing the integrated intensities and the absorbance values of the N-CD samples with the QS, the QY of the aqueous N-CDs was determined. The spectroscopic data were plotted (Fig. S1†) and the QY of the N-CDs was calculated according to the following formula:

$$QY_S = QY_R \left(\frac{Grad_S}{Grad_R}\right)\left(\frac{\eta_S^2}{\eta_R^2}\right) \quad (1)$$

where the subscripts S and R refer to the sample and reference, respectively. Grad is the gradient from the plot of integrated PL emission against absorbance, and η is the refractive index of the solvent.

2.5 Adsorption studies

The Cu(II) adsorption onto N-CDs was carried out with batch experiments. A stock solution (1000 ppm) of Cu(II) was prepared by dissolving a suitable amount of copper nitrate and then diluted with deionized water (DI). Different concentrations of adsorbate were then prepared from the stock solution by standard dilution manners. The adsorption capacities of N-CDs for Cu(II) were studied at room temperature by mixing 100 mg of N-CDs into the flasks containing 25 mL of copper ions (100 mg L^{-1}). The solutions were finally centrifuged at 2000 rpm and the supernatant then analyzed *via* atomic absorption spectroscopy (AAS). The adsorption uptake and removal

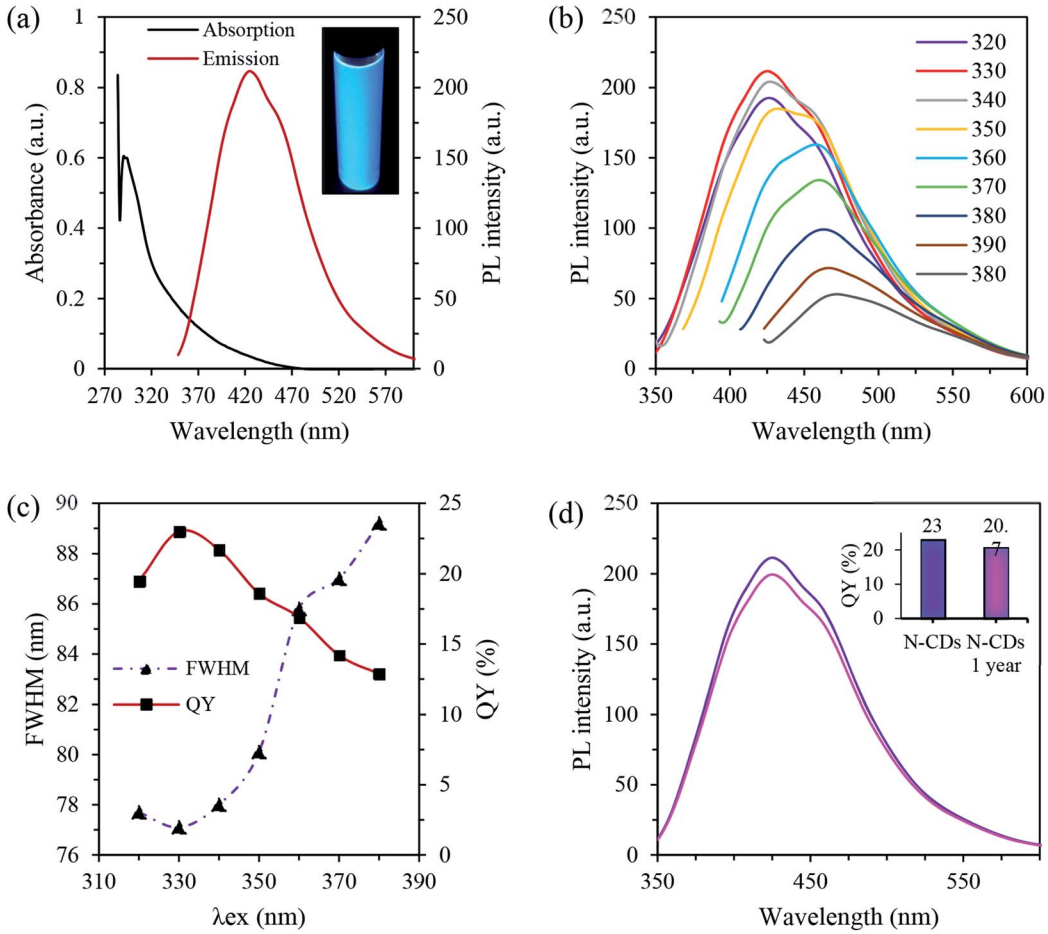

Fig. 2 Optical properties of N-CDs showing (a) absorption spectra (black line) combined with PL spectra (red line), (b) PL spectra at different excitation wavelengths, (c) emission FWHM and QY as a function of excitation wavelength and (d) freshly produced N-CDs and after 1 year storage in a dark environment. Inset in panels (a) digital photo of N-CDs under illumination of UV light at 365 nm and (d) corresponding QYs of the N-CDs.

performance of Cu(II) from wastewater were determined using the following equations:

$$q_e = \frac{(C_0 - C_e)v}{m} \quad (2)$$

$$\text{Adsorption } (\%) = \frac{C_0 - C_e}{C_0} \times 100 \quad (3)$$

where q_e is the equilibrium of Cu(II) at any time (mg g^{-1}), m (g), v (L), C_0 (mg L^{-1}) and C_e (mg L^{-1}) are the amount of N-CDs, volume of Cu(II), and initial and equilibrium concentrations of copper in solution, correspondingly.

The influence of pH, N-CD dosage, contact time and copper concentration were optimized by varying one factor while keeping others constant. In detail, the effect of pH on N-CDs was conducted in the pH range of 3–13 at room temperature with 10 mg of adsorbent dose and an initial concentration of 100 mg L^{-1} for 30 min. The optimization of dosage was performed at room temperature using 10–200 mg of N-CDs while the values of other variables were fixed at 100 mg L^{-1}, 7 and 10 min for C_0, pH and time, respectively. The influence of contact time on the copper adsorption was carried out in the range of 1–70 min (pH 7; dosage 100 mg; C_0 100 mg L^{-1}; temperature 25 °C). The impact of adsorbate concentration on their adsorption onto N-CDs was studied in the range of 20–100 mg L^{-1} (pH 7; dosage 100 mg; time 30 min; temperature 25 °C). For isotherm modeling, experiments were conducted at room temperature using different Cu(II) concentrations and optimum pH, dosage and contact time. The kinetic tests were carried out at optimum parameters and after a certain time (t) of adsorption, the concentration of Cu(II) was determined *via* AAS.

3. Results and discussion

3.1 Optimization of synthesis conditions

The QY of the N-CDs is highly altered by the processing variables like temperature, time and amino weight. Thus, several experiments were carried out to synthesize the best luminescence N-CDs from CMC and PEG as shown in Tables S1 and S2.† Under optimal conditions, N-CDs with a QY of 27% were obtained. The N-CDs with the highest QY suggest that the carbon nuclear growth and the carbonization reaction successfully completed.[30] In comparison, the QY of undoped CDs is

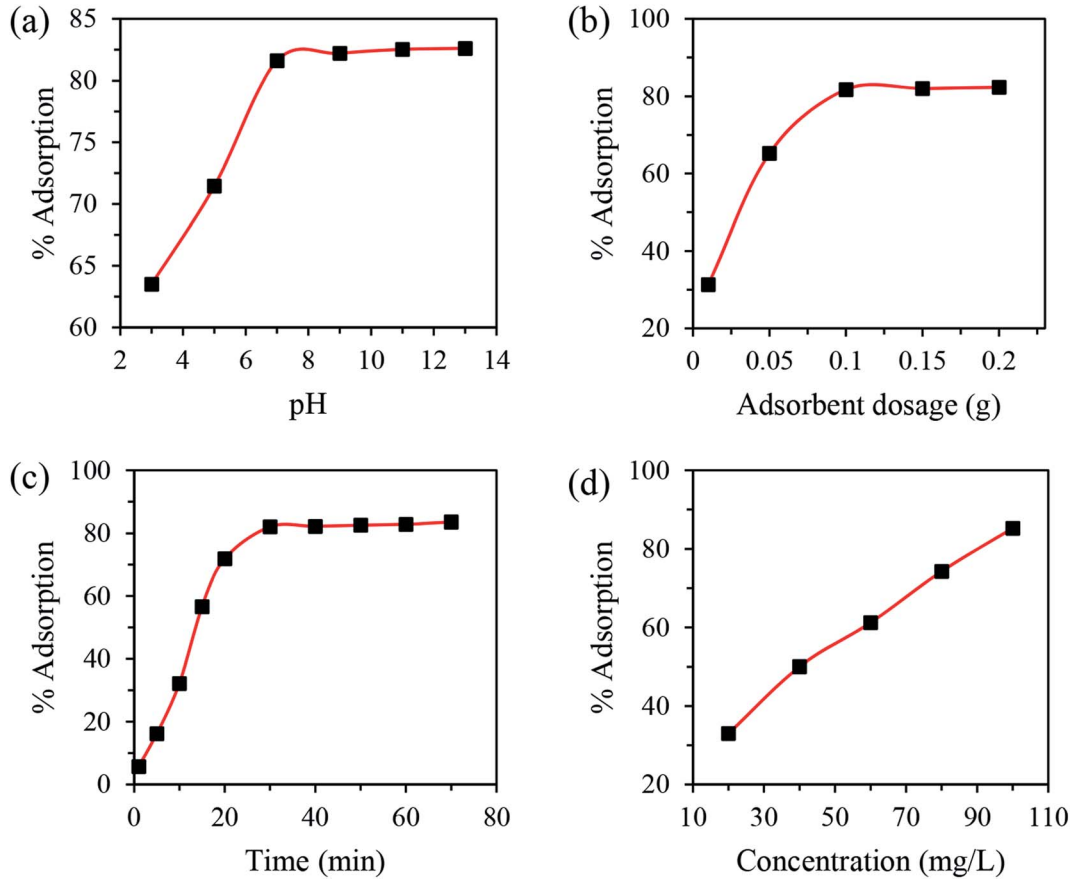

Fig. 3 Adsorption removal as a function of (a) pH, (b) adsorbent dosage, (c) contact time and (d) initial concentration.

calculated to be 7%, indicating that PEG can remarkably enhance the fluorescence emission of the CDs by introducing energy states corresponding to the N-species.[18,24] The summary presented in Table 1 demonstrates the advantageous features of the present study in terms of the mild synthetic conditions and higher QY.

A possible formation mechanism corresponding to the hydrothermal treatment of CMC and PEG is illustrated in Fig. S2.† Several reactions, including dehydration, polymerization, carbonization, and passivation, take place over the formation of N-CDs using a hydrothermal route.[34–41] First, at elevated temperatures, CMC molecules hydrolyze to form glucose. Additionally, PEG reacts with the aldehyde of glucose to form glucosamines. Amadori compounds are then produced through dehydration and fragmentation processes resulting in the formation of hydroxymethylfurfural (HMF) and the latter is rehydrated to produce organic species like levulinic acid and formic acid. Successive processes, including fragmentation, substitution, condensation, reversion, and/or dehydration, may occur to transform these by-products into polymeric compounds. A burst in the nucleation of N-CDs takes place when the concentration of the aromatic sites in the polymers reaches the critical supersaturation point. This was followed by the attachment of oxygeneous moieties such as carbonyl and dicarbonyl groups to the edge of the CDs. At the same time, amino groups penetrated the sp^2 hybridized domain to form pyridinic and graphitic N. Meanwhile, the surface of N-CDs was coated with cyclic amines. The final composition and structure of the N-CDs were further supported by TEM, HRTEM, zeta potential, EDS, FTIR and XPS.

3.2 Structural and optical properties of N-CDs

TEM and HRTEM were used to characterize the morphology and crystallinity of the sample, as displayed in Fig. 1. The TEM image in Fig. 1a shows that these nanodots are spherical and monodispersed. The HRTEM image (inset of Fig. 1a) reveals a noticeable crystalline structure with a lattice distance of 0.24 nm, assigned to the (102) facet of graphite with crystalline domains. Furthermore, the size distribution histogram of the obtained N-CDs (Fig. 1b) exhibits a narrow size distribution with an average size of 3.4 nm. The results agree with the XRD

Table 2 Isotherm parameters for Cu(II) adsorption onto N-CDs

Langmuir			Freundlich		
q_m	K_L	R^2	n	K_F	R^2
26.95	0.014	0.9983	1.63	1.04	0.9885

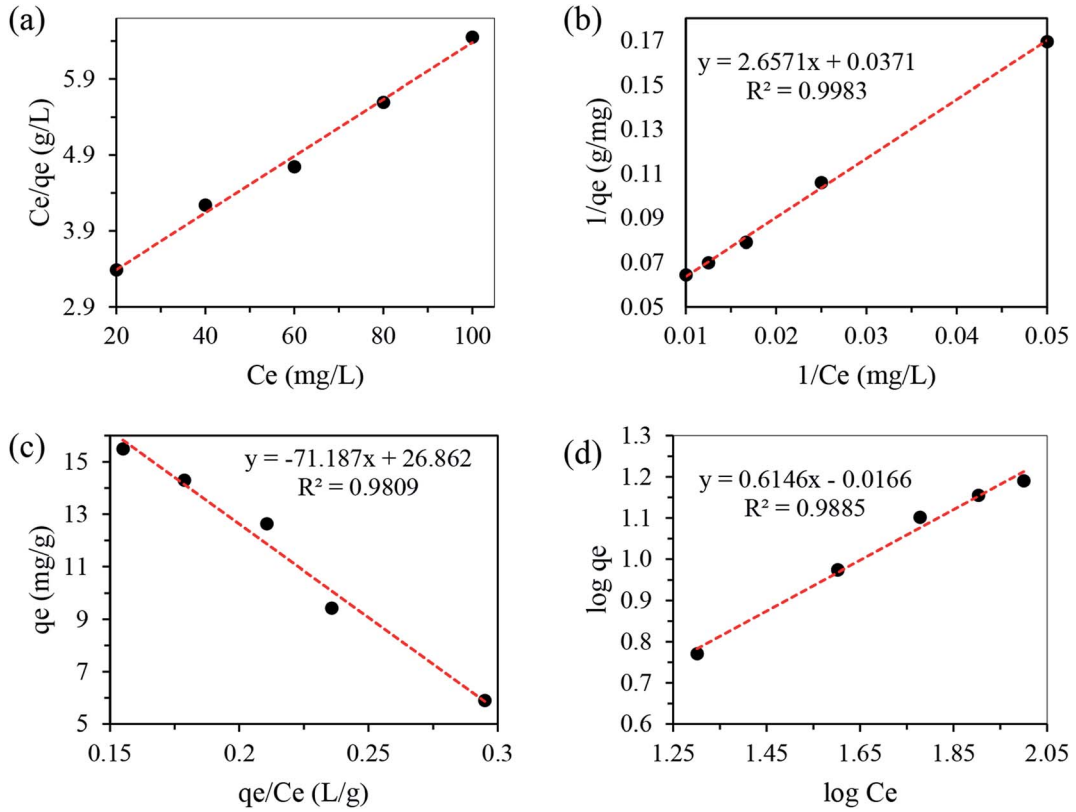

Fig. 4 Different plots of Langmuir isotherms for the adsorption of Cu(II) onto N-CDs (a–c) and Freundlich isotherm (d).

data of N-CDs (Fig. 1c) with a peak centered at $2\theta = 23.8°$, which corresponds to the diffraction of the (002) lattice spacing of carbon-based materials.[42]

Based on the results obtained by the zeta potential study (Fig. 1d), the surface charge changes from 12 mV to −38 mV with the increase of pH value from 3 to 13, demonstrating the reversible protonation and deprotonation of the active sites, including –NH and COOH, on the edge of N-CDs. The highest ξ potential of −38 was observed at pH 13, suggesting that numerous moieties exist. These negatively-charged species can act as stabilizing barriers and thus restrict the coagulation of N-CDs for a long period.[43] The ξ potential analysis showed that the synthesized N-CDs had an isoelectric point at pH 5.7. Further information on the characterization of the N-CDs together with an detailed discussion of the EDS analysis (Table S3†), FTIR results (Fig. S4†) and XPS data (Fig. S5†) can be found in the ESI† (Section II).

The optical properties of the N-CDs were studied with UV-vis absorption and PL spectroscopy. The optical absorption spectra of N-CDs display intense peaks in the UV region at 284 nm and a tail extended in the visible region, which is attributed to the n–π^* transition of the C=O/C=N groups and π–π^* transition of the aromatic sp^2 framework, respectively (Fig. 2a).[32,44] The obtained N-CDs exhibited bright blue emission under the irradiation of a UV light source exciting at 365 nm (the inset of Fig. 2a). Moreover, the optimal luminescence was noticed at 431 nm when excited at 330 nm, suggesting that the largest number of nanodots are excited at that wavelength.[45] The N-CDs had a Stokes shift of 101 nm, which is an advantage for bio-imaging applications.[16]

Fig. 2b presents the PL emission spectra of N-CDs at different excitation wavelengths. Two behaviors could be shown where excitation independent emission was observed in the range of 310–320 nm excitation and an excitation dependent emission from 330 to 380 nm excitation. The XPS, FTIR and absorption spectra of the N-CDs shown earlier agree well with the results obtained from the PL spectra. More specifically, the higher absorption peak at 284 nm confirms the energy transition from the HOMO to the LUMO originating in the carbon

Table 3 Comparison of different adsorbents for Cu(II) removal[a]

Adsorbent	Time consumed (min)	q_m (mg g^{-1})	Ref.
Pomegranate wood AC	43.1	1.683	2
Vegetable waste AC	90	75	52
Wheat shell	180	17.42	53
OPEFB AC	—	0.84	54
Sewage sludge AC	60	7.73	51
Palm shell AC	20	18.6	55
Wheat shell	120	10.84	56
Hazelnut shell	120	6.74	57
Lignocellulosic waste N-CDs	30	26.95	This work

[a] AC: activated carbon; OPEFB: oil palm empty fruit bunch.

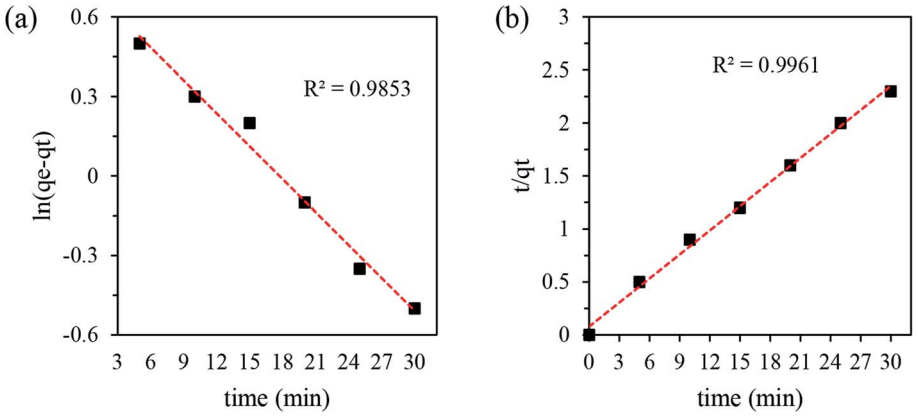

Fig. 5 (a) Pseudo-first order kinetics fit (b) pseudo-second order kinetics fit, (c) effect of a series of scavengers on the desorption of Cu^{2+} from N-CDs and (d) the reusability of the N-CDs in Cu^{2+} removal from an aqueous suspension for five cycles with the optimized sample.

core (C–C and graphitic N), leading to the excitation independent emission due to the absence of multiple PL centers.[46] Meanwhile, the lower energy absorption tail is related to the transition from the HOMO to the LUMO of the surface state (pyridine N, amino N, and C=O groups). The latter can create a series of defect levels in the bandgap, resulting in the excitation dependent emission. Hence the PL emission of N-CDs is tuned by both the size and surface defects.

Fig. 2c illustrates the full width at half maximum (FWHM) of the emission spectra as a function of excitation wavelength. A slight change of excitation wavelength in the range of 320–350 nm was observed with a minimum FWHM of 77.1 nm at λ_{ex} = 330 nm. However, an increase in the FWHM was shown when the excitation value was higher than 350 nm. This demonstrates the suitability of using these nanomaterials in a broad range of analytical applications.[47] Moreover, Fig. 2c shows that the QY was dependent on the excitation values. In detail, the rise in the QY occurred with the increase of excitation wavelength, reaching a maximum of ~23% at 330 nm excitation. However, a further increase of excitation values has a negative influence on the QY. Comparing the dependence of QY and FWHM suggests a trade-off exists between the QY and FWHM.

Moreover, no significant loss of PL emission (Fig. 2d) was observed even after being stored for 1 year in a room under ambient conditions. The inset in Fig. 2d shows the QYs of N-CDs as a function of 1 year storage, in which a QY retention of around 97.7% was noticed compared to the freshly synthesized N-CD suspension. The long-term storage stability demonstrates that N-CDs are a suitable candidate for biological functions.

3.3 Optimization of adsorption parameters

3.3.1 Effect of pH. The effect of pH in the range of 3–13 on the adsorption of Cu(II) using N-CDs was investigated as illustrated in Fig. 3a. It can be seen that the adsorption capacity increases with increasing pH from 3 to 7 and reaches the maximum when the pH is at 7, in which a further increase of pH causes no significant removal of Cu(II). In acidic pH, the adsorption uptake of Cu(II) is low owing to the release of H_3O^+ ions. These ions compete with Cu(II) for the active sites on the surface of N-CDs, leaving Cu(II) free in the solution.[48,49] With increasing pH until 7, the surface occupation declines and positively charged Cu(II) attach to the free active sites of the adsorbent.[1] As previously reported, metal ion adsorption is favorable at a suspension pH higher than the pH_{PZC} values.[48] The ξ potential data (Fig. 1d) agrees well with pH results, in which after the isoelectric point at pH 5.7, the negative charge containing groups become dominant. As a consequence, electrostatic attraction occurs between Cu(II) and the N-CD surface, leading to an improvement of adsorption uptake. Thus, pH = 7 was chosen as the optimal value for subsequent experiments owing to the negative charges on the adsorbent edge.

3.3.2 Effect of dose. Keeping in mind the importance to achieve the optimal removal capacity with as low an adsorbent dose as possible, the optimization of dosage was performed in the range of 10–200 mg while the other variables were fixed at 100 mg L^{-1}, 7 and 30 min for C_0, pH and time, respectively. Fig. 3b shows the percentage adsorption as a function of dose. As the adsorbent dose increased from 10 to 100 mg, an enhancement in the % adsorption from 31 to 81.76% was noticed. The reason for this can be explained as follows: as the dose increases from zero, many more active sites are available, resulting in the enhancement of Cu(II) adsorbed. Yet, when the dose is too high, it is believed that the aggregation of the adsorbent particles occurs, leading to the reduction in the adsorption as a result of reducing the surface area.[49] Therefore, 100 mg of N-CDs was considered the optimum dosage.

3.3.3 Effect of contact time. The influence of contact time on the adsorption removal of Cu(II) using N-CD as an adsorbent

Table 4 Kinetic model parameters for copper adsorption onto N-CDs

Pseudo-first order			Pseudo-second order		
q_e	K_1	R^2	q_e	K_2	R^2
5.4	0.1	0.9853	13.2	0.075	0.9961

was studied over time from 1 to 70 min. As shown in Fig. 3c, two stages were observed: rapid Cu(II) adsorption achieving 82.1% within 30 min and relatively slow adsorption increasing to 83.6% over the adsorption time of 30 to 70 min. However, the latter improved adsorption was insignificant. The trend observed in this study was consistent with that of the reported work using CDs as an adsorbent[50] and consequently, the best duration of time for Cu(II) adsorption onto N-CDs was noted to be 30 min. In comparison to other adsorbents reported in the literature,[2,49] our present work is superior in terms of equilibrium time, which is suitable for practical applications.

3.3.4 Effect of initial concentration. The influence of the initial concentration of Cu(II) on the percentage adsorption of N-CDs was evaluated at ambient temperature using different concentrations in the range of 20–100 mg L^{-1}. Fig. 3d shows that the removal efficiency rises with increasing initial Cu(II) concentration. This enhanced adsorption with rising concentrations could be assigned to a greater driving force for mass transfer from the suspension to the edge of N-CDs.[49] Therefore, 100 mg L^{-1} was selected as the optimum value for the following tests.

3.4 Modeling

3.4.1 Adsorption isotherm. The adsorbate–adsorbent binding can be clearly understood by studying the fit of the Langmuir and Freundlich isotherm models. Detailed information on the two models is presented in the ESI† (Section III). The isotherm models were studied under the optimal conditions at room temperature. The results of the corresponding numerical parameters are summarized in Table 2. The Langmuir parameters were evaluated using three forms of Langmuir isotherms (Fig. 4a–c). There is an adequate fit for the first and second Langmuir plots with an R^2 of 0.9935 and 0.9983, respectively, as compared to the third plot ($R^2 = 0.9809$). However, the results suggest that the Langmuir isotherm fits better than the Freundlich isotherm (Fig. 4d) under the concentration range tested. This may be attributed to the homogeneous distribution of functional groups on the N-CD edges since the Langmuir model assumes that the surface is homogenous.[51] The maximum adsorption uptake for copper onto N-CDs is determined to be 26.95 mg g^{-1}. To compare the adsorption uptake of N-CDs with other adsorbents, a summary of adsorbents for

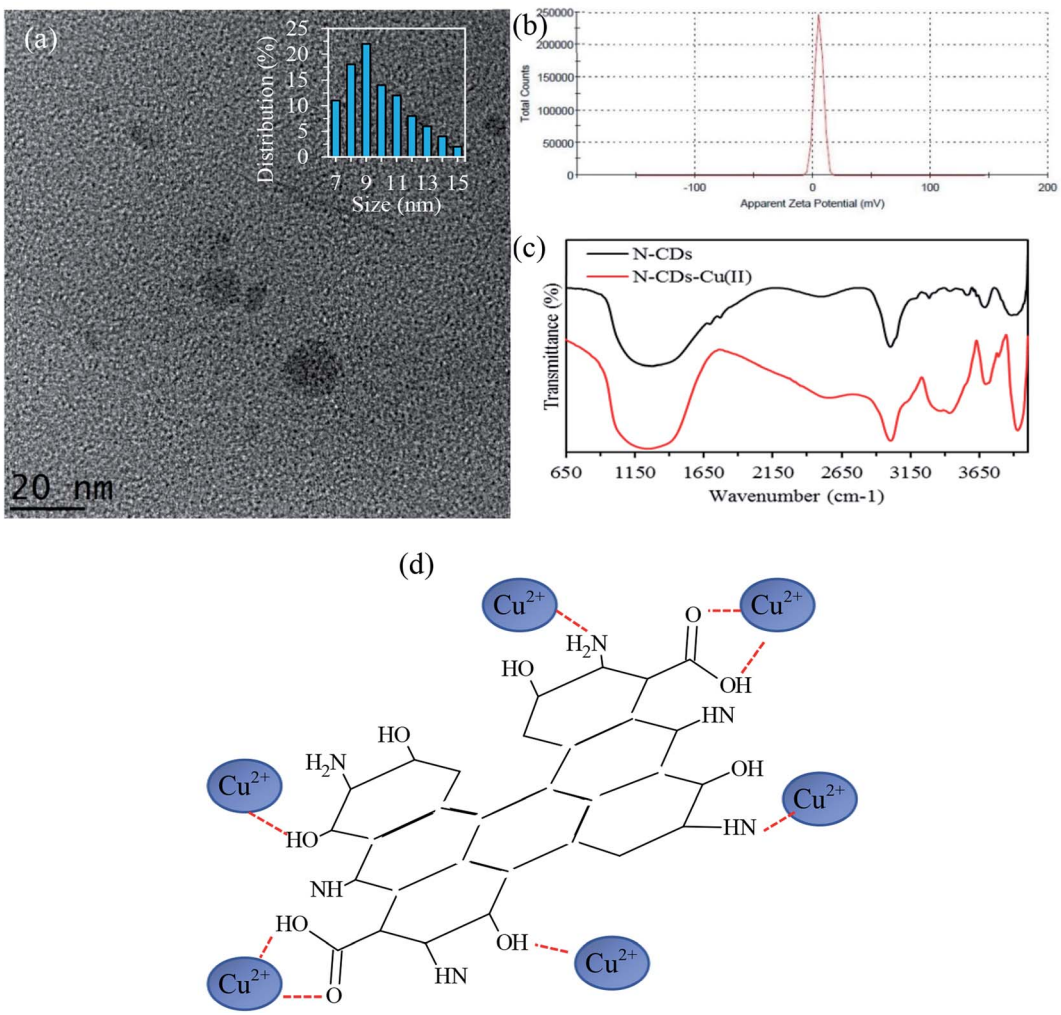

Fig. 6 (a) TEM image, (b) zeta potential, (c) FTIR of N-CD suspension in the presence of copper ions and (d) possible adsorption mechanism of Cu(II) onto the N-CD edge. Inset of (a) shows the size distribution.

Cu(II) removal is illustrated in Table 3. The favorable adsorption was noticed since the values of R_L were between 0 and 1.

3.4.2 Adsorption kinetic model. The kinetics of the adsorption reaction are significant in wastewater remedy as it reveals critical information about the nature of the adsorbent materials and the dynamic process. Thus, the adsorption mechanism of Cu(II) was studied by assessing both pseudo first-order and second-order kinetic models, which can be explained as follows:pseudo-first order kinetic model

$$\log(q_e - q_t) = \log q_e - (k_1/2.303)t \quad (4)$$

pseudo-second order kinetic model

$$\frac{t}{q_t} = \frac{1}{k_2 q_e^2} + \frac{t}{q_e} \quad (5)$$

where q_t (mg g^{-1}) and q_e (mg g^{-1}) are the adsorption uptake at time t and equilibrium, respectively. k_1 (min^{-1}) and k_2 (g(mg min^{-1})) are the rate constants of the pseudo-first-order and pseudo-second-order models.

The kinetics data were calculated from the slope and intercepts of the straight–line curves of $\ln(q_e - q_t)$ *versus* (t) (Fig. 5a) for the pseudo-first-order model and t/q_t *versus* (t) (Fig. 5b) for the pseudo-second-order model, and the results are listed in Table 4. The adequacy of the models was determined by comparing the correlation coefficient (R^2) of the two models. The pseudo-second-order kinetic model with $R^2 = 0.9961$ for copper was higher than that of the pseudo-first-order kinetics model ($R^2 = 0.9853$). Hence, the chemisorption of the adsorption process follows pseudo-second order kinetics behavior.

3.4.3 Adsorption mechanism investigation. Despite the effective and rapid adsorption uptake that can be achieved using N-CDs, there are insufficient reports on the adsorption mechanism of metal ions onto fluorescent nano-adsorbents. Thus, several spectroscopic analyses were performed to gain better insight into the copper removal by N-CDs. In comparison to the TEM imaging of the pure N-CD suspension, a remarkable rise in the size of the N-CDs-Cu^{2+} complex was noticed (Fig. 6a). The size distribution curve was in the range of 7–15 nm for the complex with an average diameter of 8.6 nm, which is bigger than that of N-CDs (range of 3–8 nm and 3.4 nm diameter). This provides evidence for the aggregation of N-CDs through the formation of N-CDs-Cu^{2+} complexes.[58–60] Following this, the ξ potential value of 5.08 eV was measured after the addition of Cu^{2+} (Fig. 6b). In comparison to the ξ potential of pure N-CDs at pH 7, this rise in ξ potential suggested that the charges of N-CDs were neutralized by the positive charges of Cu^{2+} due to the electrostatic effect.[7]

FTIR spectroscopy (Fig. 6c) was also conducted to investigate the interaction of copper with N-CDs. In comparison to the pure

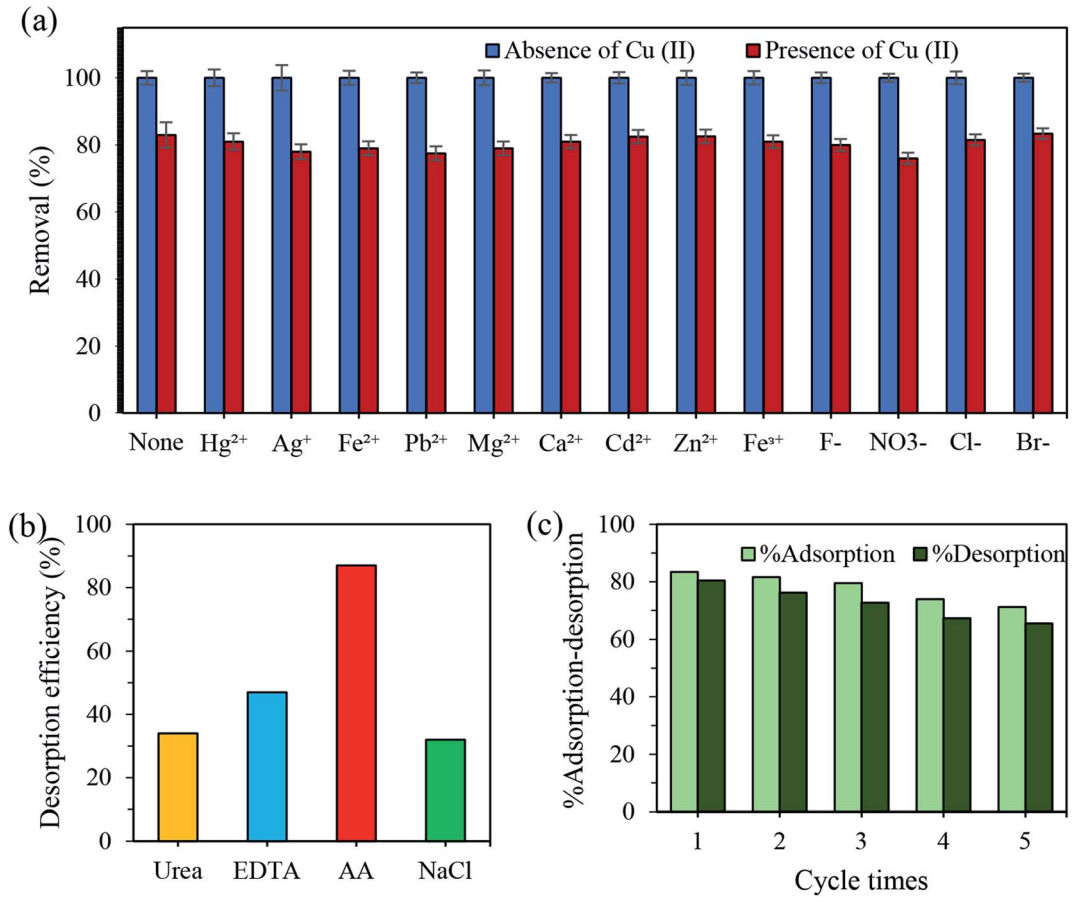

Fig. 7 (a) Effects of inorganic species on the adsorption of N-CDs for Cu^{2+}; dosage 0.1 g, concentration 100 ppm, pH 7.4 ± 0.1, time 30 min. (b) Reversible study of N-CDs towards Cu(II).

N-CDs, there is a large increase and red-shift of the C–N band from 1266 cm^{-1} to 1214 cm^{-1} after adding Cu^{2+}. This could be assigned to the binding affinity of N to Cu^{2+} that weakens the C–N bond and thus vibrates at a lower energy.[61] In addition, the increase in the peak intensity at 725 cm^{-1} may be ascribed to the coordinate bond formation between the hydrogen atom of the methyl groups and the copper center. In detail, the strong hydrogen bonds between water molecules and carboxylate groups and the anagostic interactions between C–H···Cu is clear evidence of the formation of the intramolecular complex.[62,63] Furthermore, the stretching vibrations of C=O, C–O and C–O–C at 1641, 1045 and 1016 cm^{-1}, respectively, were significantly affected after Cu^{2+} addition. This could be due to the coordinate bond formation between Cu^{2+} and the active sites around N-CDs. It is believed that O atoms can donate a lone pair of electrons to the Cu^{2+}, forming a coordinate covalent bond between Cu^{2+} and O owing to the high oxidability of copper.[64–67] Considering the above results, the proposed Cu(II) adsorption by N-CDs was illustrated in Fig. 6d, in which a N-CDs-Cu^{2+} complex was formed due to the electrostatic interaction between Cu(II) and the $–COO^-$, –OH and –N functional sites on the surface of N-CDs.

3.4.4 Performance evaluation. With inherent pollution, metal ion adsorption in aqueous media has superior advantages in practical application in terms of selectivity. In this regard, the interference effect of various cations (Hg^{2+}, Ag^+, Fe^{2+}, Pb^{2+}, Mg^{2+}, Ca^{2+}, Cd^{2+}, Zn^{2+}, and Fe^{3+}) and anions (F^-, NO_3^-, Cl^-, and Br^-) on the adsorption process of Cu^{2+} was investigated. All the inorganic moieties were performed in PBS (pH 7.4) at a concentration of 100 ppm along with 100 ppm of Cu^{2+}. As presented in Fig. 7a, no significant reduction in the adsorption rate (<5.5%) for Cu^{2+} removal was noticed after adding different inorganic moieties, demonstrating the nearly zero coordination of active sites to most co-existing cations and anions.

The reusability and regeneration ability of the adsorbent was also investigated to evaluate its performance for practical applications. First, the recycling tests to recover the adsorbed Cu(II) were carried out using urea (0.1 M), EDTA (0.1 M), AA (0.1 M) and NaCl (0.1 M). The results demonstrated the great effectiveness of AA to desorb Cu(II) from N-CDs (Fig. 7b). Next, the regeneration experiments were conducted using AA as a reducing agent. As shown in Fig. 7c, there is no significant reduction of the percent adsorption even after five adsorption–desorption cycles, in which only a 14.95% loss in the removal efficiency of the recycled material was observed. The loss in % adsorption might be assigned to the loss of the adsorbent or the irreversible occupation of some of the adsorption sites.[68] The above results indicated the ability of AA to reduce the Cu^{2+}-N-CDs nanocomplex into Cu^+ ions.[69,70] The excellent reusability suggested that the obtained N-CDs adsorbent could be potentially used for practical wastewater treatment.

4. Conclusion

In this work, we developed a versatile method to produce highly luminescent N-CDs using CMC and PEG as precursors. The characterization results reveal that the formed N-CDs have an average particle diameter of 3.4 nm. The optimal N-CDs show high crystallinity, a surface coated by the amino moieties of PEG and an enhanced QY of up to 27%. The adsorption test shows that the best conditions for the maximum removal of Cu(II) using N-CDs were: pH 7; dose 100 mg; time 30 min; and concentration 100 mg L^{-1}. Under optimal variables, an adsorption capacity of 26.95 mg g^{-1} was obtained. Isotherm and kinetic studies indicate that the adsorption reaction was described well by the Langmuir and pseudo-second-order model, respectively. Moreover, the excellent reusability of the adsorbent was obtained by the adsorption–desorption test. Therefore, the work demonstrated the suitability of using N-CDs as an effective adsorbent for the treatment of polluted water containing toxic copper ions.

Conflicts of interest

The authors declare that there is no conflict of interest regarding the publication of this work.

Acknowledgements

The authors would like to thank Universiti Putra Malaysia, Malaysia as this reported research work is funded by the UPM under the GP-IPS/2017/9556800 grant.

References

1 P. Kahrizi, F. S. Mohseni-Shahri and F. Moeinpour, Adsorptive removal of cadmium from aqueous solutions using $NiFe_2O_4$/hydroxyapatite/graphene quantum dots as a novel nano-adsorbent, *J. Nanostruct. Chem.*, 2018, **8**(4), 441–452.
2 A. M. Ghaedi, *et al.*, Adsorption of copper (II) using modified activated carbon prepared from Pomegranate wood: Optimization by bee algorithm and response surface methodology, *J. Mol. Liq.*, 2015, **206**, 195–206.
3 V. V. N. Singh, *et al.*, Sensitive and selective detection of copper ions using low cost nitrogen doped carbon quantum dots as a fluorescent sensing plateform, *ISSS Journal of Micro and Smart Systems*, 2017, **6**(2), 109–117.
4 B. K. Bansod, T. Kumar, R. Thakur, S. Rana and I. Singh, A review on various electrochemical techniques for heavy metal ions detection with different sensing platforms, *Biosens. Bioelectron.*, 2017, **94**, 443–455.
5 P. Kumar, K.-H. Kim, V. Bansal, T. Lazarides and N. Kumar, Progress in the sensing techniques for heavy metal ions using nanomaterials, *J. Ind. Eng. Chem.*, 2017, **54**, 30–43.
6 L. Basabe-Desmonts, D. N. Reinhoudt and M. Crego-Calama, Design of fluorescent materials for chemical sensing, *Chem. Soc. Rev.*, 2007, **36**(6), 993–1017.
7 M. A. Issa, *et al.*, Facile Synthesis of Nitrogen-Doped Carbon Dots from Lignocellulosic Waste, *Nanomaterials*, 2019, **9**(10), 1500.
8 S. Y. Lim, W. Shen and Z. Gao, Carbon quantum dots and their applications, *Chem. Soc. Rev.*, 2015, **44**(1), 362–381.
9 Y. Chan, J. Chen, Q. Liu, S. E. Wark, D. H. Son and J. D. Batteas, Ultrasensitive Copper (II) Detection Using

Luminescence of CdSe Quantum Dots, *Anal. Chem.*, 2010, **82**(9), 3671–3678.
10 R. Zhang and W. Chen, Nitrogen-doped carbon quantum dots: Facile synthesis and application as a 'turn-off' fluorescent probe for detection of Hg^{2+} ions, *Biosens. Bioelectron.*, 2013, **55**, 83–90.
11 Z. Xu, J. Yu and G. Liu, Fabrication of carbon quantum dots and their application for efficient detecting $Ru(bpy)_3^{2+}$ in the solution, *Sens. Actuators, B*, 2013, **181**, 209–214.
12 S. Y. Lim, W. Shen and Z. Gao, Carbon quantum dots and their applications, *Chem. Soc. Rev.*, 2014, **44**(1), 362–381.
13 A. M. Derfus, W. C. W. Chan and S. N. Bhatia, Probing the Cytotoxicity of Semiconductor Quantum Dots, *Nano Lett.*, 2004, **4**(1), 11–18.
14 X. T. Zheng, A. Ananthanarayanan, K. Q. Luo and P. Chen, Glowing Graphene Quantum Dots and Carbon Dots: Properties, Syntheses, and Biological Applications, *Small*, 2015, **11**(14), 1620–1636.
15 H. Liu, *et al.*, High-Efficient Excitation-Independent Blue Luminescent Carbon Dots, *Nanoscale Res. Lett.*, 2017, **12**, 0–6.
16 G. Ren, *et al.*, One pot synthesis of highly fluorescent N doped C-dots and used as fluorescent probe detection for Hg^{2+} and Ag^{+} in aqueous solution, *Sens. Actuators, B*, 2017, **243**, 244–253.
17 X. Sun and Y. Lei, Fluorescent carbon dots and their sensing applications, *TrAC, Trends Anal. Chem.*, 2017, **89**, 163–180.
18 L. Li and T. Dong, Photoluminescence Tuning in Carbon Dots: Surface Passivation or/and Functionalization, Heteroatom Doping, *J. Mater. Chem. C*, 2018, **6**(30), 7944–7970.
19 T. T. Meiling, *Development of a reliable and environmentally friendly synthesis for fluorescence carbon nanodots*, University of Potsdam, 2017.
20 M. C. Ortega-Liebana, *et al.*, Uniform luminescent carbon nanodots prepared by rapid pyrolysis of organic precursors confined within nanoporous templating structures, *Carbon*, 2017, **117**, 437–446.
21 S. Mohapatra, S. Sahu, N. Sinha and S. K. Bhutia, Synthesis of a carbon-dot-based photoluminescent probe for selective and ultrasensitive detection of Hg^{2+} in water and living cells, *Analyst*, 2015, **140**(4), 1221–1228.
22 L. Hu, *et al.*, Multifunctional carbon dots with high quantum yield for imaging and gene delivery, *Carbon*, 2013, **67**, 508–513.
23 T. Kavitha and S. Kumar, Turning date palm fronds into biocompatible mesoporous fluorescent carbon dots, *Sci. Rep.*, 2018, **8**(1), 1–10.
24 V. Arul and M. G. Sethuraman, Facile green synthesis of fluorescent N-doped carbon dots from Actinidia deliciosa and their catalytic activity and cytotoxicity applications, *Opt. Mater.*, 2018, **78**, 181–190.
25 Q. Wu, W. Li, J. Tan, Y. Wu and S. Liu, Hydrothermal carbonization of carboxymethylcellulose: One-pot preparation of conductive carbon microspheres and water-soluble fluorescent carbon nanodots, *Chem. Eng. J.*, 2015, **266**, 112–120.
26 P. Shen, J. Gao, J. Cong, Z. Liu, C. Li and J. Yao, Synthesis of Cellulose-Based Carbon Dots for Bioimaging, *ChemistrySelect*, 2016, **1**(7), 1314–1317.
27 S. Jayaweera, K. Yin, X. Hu and W. J. Ng, Facile preparation of fluorescent carbon dots for label-free detection of Fe^{3+}, *J. Photochem. Photobiol., A*, 2019, **370**, 156–163.
28 P. Shen, J. Gao, J. Cong, Z. Liu, C. Li and J. Yao, Synthesis of Cellulose-Based Carbon Dots for Bioimaging, *ChemistrySelect*, 2016, **1**(7), 1314–1317.
29 Q. Wu, W. Li, J. Tan, Y. Wu and S. Liu, Hydrothermal carbonization of carboxymethylcellulose: One-pot preparation of conductive carbon microspheres and water-soluble fluorescent carbon nanodots, *Chem. Eng. J.*, 2015, **266**, 112–120.
30 M. Abdullah Issa, *et al.*, Fabrication, characterization and response surface method optimization for quantum efficiency of fluorescent nitrogen-doped carbon dots obtained from carboxymethylcellulose of oil palms empty fruit bunch, *Chin. J. Chem. Eng.*, 2019, DOI: 10.1016/j.cjche.2019.04.003.
31 P. Wu, W. Li, Q. Wu, Y. Liu and S. Liu, Hydrothermal synthesis of nitrogen-doped carbon quantum dots from microcrystalline cellulose for the detection of Fe^{3+} ions in an acidic environment, *RSC Adv.*, 2017, **7**(70), 44144–44153.
32 S. Jayaweera, K. Yin, X. Hu and W. J. Ng, Fluorescent N/Al Co-Doped Carbon Dots from Cellulose Biomass for Sensitive Detection of Manganese (VII), *J. Fluoresc.*, 2019, **29**, 1291–1300.
33 G. Yang, X. Wan, Y. Su, X. Zeng and J. Tang, Acidophilic S-doped carbon quantum dots derived from cellulose fibers and their fluorescence sensing performance for metal ions in an extremely strong acid environment, *J. Mater. Chem. A*, 2016, **4**(33), 12841–12849.
34 M. Sevilla and A. B. Fuertes, The production of carbon materials by hydrothermal carbonization of cellulose, *Carbon*, 2009, **47**(9), 2281–2289.
35 K. Yu, J. Wang, K. Song, X. Wang, C. Liang and Y. Dou, Hydrothermal Synthesis of Cellulose-Derived Carbon Nanospheres from Corn Straw as Anode Materials for Lithium ion Batteries, *Nanomaterials*, 2019, **9**(1), 93.
36 E. García-Bordejé, E. Pires and J. M. Fraile, Parametric study of the hydrothermal carbonization of cellulose and effect of acidic conditions, *Carbon*, 2017, **123**, 421–432.
37 R. Li, L. Wang and A. Shahbazi, A Review of Hydrothermal Carbonization of Carbohydrates for Carbon Spheres Preparation, *Trends Renew. Energ.*, 2015, **1**(1), 43–56.
38 C. Falco, N. Baccile and M. M. Titirici, Morphological and structural differences between glucose, cellulose and lignocellulosic biomass derived hydrothermal carbons, *Green Chem.*, 2011, **13**(11), 3273–3281.
39 N. R. Pires, C. M. W. Santos, R. R. Sousa, R. C. M. De Paula, P. L. R. Cunha and J. P. A. Feitosa, Novel and fast microwave-assisted synthesis of carbon quantum dots from raw cashew gum, *J. Braz. Chem. Soc.*, 2015, **26**(6), 1274–1282.
40 W. J. Niu, Y. Li, R. H. Zhu, D. Shan, Y. R. Fan and X. J. Zhang, Ethylenediamine-assisted hydrothermal synthesis of nitrogen-doped carbon quantum dots as fluorescent probes for sensitive biosensing and bioimaging, *Sens. Actuators, B*, 2015, **218**, 229–236.

41 A. Schmidt, M. Schneiders, M. Döpfner and G. Lehmkuhl, Theory, Production and Mechanism of Formation of Monodispersed Hydrosols, *J. Am. Chem. Soc.*, 1950, **72**(3), 4847–4854.

42 F. Wu, H. Su, K. Wang, W. K. Wong and X. Zhu, Facile synthesis of N-rich carbon quantum dots from porphyrins as efficient probes for bioimaging and biosensing in living cells, *Int. J. Nanomed.*, 2017, **12**, 7375–7391.

43 Y. Xu, D. Li, M. Liu, F. Niu, J. Liu and E. Wang, Enhanced-quantum yield sulfur/nitrogen co-doped fluorescent carbon nanodots produced from biomass Enteromorpha prolifera: synthesis, posttreatment, applications and mechanism study, *Sci. Rep.*, 2017, **7**, 4499.

44 N. Chaudhry, P. K. Gupta, S. Eremin and P. R. Solanki, One-step green approach to synthesize highly fluorescent carbon quantum dots from banana juice for selective detection of copper ions, *J. Environ. Chem. Eng.*, 2020, **8**(3), 103720.

45 L. Adinarayana, *et al.*, Single Step Synthesis of Carbon Quantum Dots from Coconut Shell: Evaluation for Antioxidant Efficacy and Hemotoxicity, *J. Mater. Sci. Appl.*, 2017, **3**(6), 83–93.

46 J. Yu, *et al.*, Luminescence mechanism of carbon dots by tailoring functional groups for sensing Fe^{3+} ions, *Nanomaterials*, 2018, **8**(4), 1–12.

47 Y. Wang, Y. Zhu, S. Yu and C. Jiang, Fluorescent carbon dots: rational synthesis, tunable optical properties and analytical applications, *RSC Adv.*, 2017, **7**, 40973–40989.

48 S. Biswas, B. C. Meikap and T. K. Sen, Adsorptive Removal of Aqueous Phase Copper (Cu^{2+}) and Nickel (Ni^{2+}) Metal Ions by Synthesized Biochar–Biopolymeric Hybrid Adsorbents and Process Optimization by Response Surface Methodology (RSM), *Water, Air, Soil Pollut.*, 2019, **230**(8), DOI: 10.1007/s11270-019-4258-y.

49 M. Alsuhybani, A. Alshahrani, M. Algamdi, A. A. Al-Kahtani and A. A. Alqadami, Highly efficient removal of Pb(II) from aqueous systems using a new nanocomposite: Adsorption, isotherm, kinetic and mechanism studies, *J. Mol. Liq.*, 2020, **301**, 112393.

50 A. Eslami, S. M. Borghei, A. Rashidi and A. Takdastan, Preparation of activated carbon dots from sugarcane bagasse for naphthalene removal from aqueous solutions, *Sep. Sci. Technol.*, 2018, **53**(16), 2536–2549.

51 X. Wang, *et al.*, Adsorption of Copper (II) onto activated carbons from sewage sludge by microwave-induced phosphoric acid and zinc chloride activation, *Desalination*, 2011, **278**(1–3), 231–237.

52 M. I. Sabela, *et al.*, Removal of copper (II) from wastewater using green vegetable waste derived activated carbon: An approach to equilibrium and kinetic study, *Arabian J. Chem.*, 2019, **12**(8), 4331–4339.

53 H. Aydın, Y. Bulut and Ç. Yerlikaya, Removal of copper (II) from aqueous solution by adsorption onto low-cost adsorbents, *J. Environ. Manage.*, 2008, **87**(1), 37–45.

54 R. Wahi, Z. Ngaini and V. Jok, Removal of mercury, lead and copper from aqueous solution by activated carbon of palm oil empty fruit bunch, *World Appl. Sci. J.*, 2009, **5**, 84–91.

55 G. Issabayeva, M. K. Aroua and N. M. Sulaiman, Study on palm shell activated carbon adsorption capacity to remove copper ions from aqueous solutions, *Desalination*, 2010, **262**(1–3), 94–98.

56 N. Basci, E. Kocadagistan and B. Kocadagistan, Biosorption of copper (II) from aqueous solutions by wheat shell, *Desalination*, 2004, **164**(2), 135–140.

57 T. Altun and E. Pehlivan, Removal of Copper(II) Ions from Aqueous Solutions by Walnut-, Hazelnut- and Almond-Shells, *Clean: Soil, Air, Water*, Dec. 2007, **35**(6), 601–606.

58 R. V. Nair, R. T. Thomas, V. Sankar, H. Muhammad, M. Dong and S. Pillai, Rapid, Acid-Free Synthesis of High-Quality Graphene Quantum Dots for Aggregation Induced Sensing of Metal Ions and Bioimaging, *ACS Omega*, 2017, **2**(11), 8051–8061.

59 L. Minh, T. Phan, S. Hoon, T. Phan, K. Yeol and S. Ha, Synthesis of fluorescent silicon quantum dots for ultra-rapid and selective sensing of Cr(VI) ion and biomonitoring of cancer cells, *Mater. Sci. Eng., C*, 2018, **93**, 429–436.

60 A. Stafiej and K. Pyrzynska, Adsorption of heavy metal ions with carbon nanotubes, *Sep. Purif. Technol.*, 2007, **58**(1), 49–52.

61 M. Ganiga and J. Cyriac, Understanding the Photoluminescence Mechanism of Nitrogen-Doped Carbon Dots by Selective Interaction with Copper Ions, *ChemPhysChem*, 2016, **17**(5), 2315–2321.

62 A. T. Çolak, O. Z. Yeilel and O. Büyükgüngör, A novel anagostic C-H···Cu interaction and clustered water molecules in copper(II)-pyridine-2,5-dicarboxylate complex, *J. Mol. Struct.*, 2011, **991**(1–3), 68–72.

63 A. Colombo, *et al.*, Intriguing C–H···Cu interactions in bis-(phenanthroline)Cu(i) redox mediators for dye-sensitized solar cells, *Dalton Trans.*, 2018, **47**(4), 1018–1022.

64 M. N. A. Al-Jibouri, S. A. H. Al-Ameri, W. M. Al-Jibouri and M. A. K. Al-Souz, Spectroscopic study of the effect of a new metal chelate on the stability of PVC, *J. Assoc. Arab Univ. Basic Appl. Sci.*, 2013, **14**(1), 67–74.

65 G. J. Ru, Q. Xin, J. X. Rui and H. Shah, Single precursor-based luminescent nitrogen-doped carbon dots and their application for iron (III) sensing, *Arabian J. Chem.*, 2019, **12**(7), 1083–1091.

66 A. Zhu, Q. Qu, X. Shao, B. Kong and Y. Tian, Carbon-Dot-Based Dual-Emission Nanohybrid Produces a Ratiometric Fluorescent Sensor for In Vivo Imaging of Cellular Copper Ions, *Angew. Chem., Int. Ed.*, 2012, **51**(29), 7185–7189.

67 Y. Liu, *et al.*, The synthesis of water-dispersible zinc doped $AgInS_2$ quantum dots and their application in Cu^{2+} detection, *J. Lumin.*, 2017, **192**, 547–554.

68 S. R. Anand, *et al.*, Antibacterial Nitrogen-doped Carbon Dots as a Reversible 'fluorescent Nanoswitch' and Fluorescent Ink, *ACS Omega*, 2019, **4**(1), 1581–1591.

69 G. Kalaiyarasan, J. Joseph and J. Joseph, Efficient dual-mode colorimetric/fluorometric sensor for the detection of copper ions and vitamin C based on pH-sensitive amino-terminated nitrogen-doped carbon quantum dots: effect of reactive oxygen species and antioxidants, *Anal. Bioanal. Chem.*, 2019, **411**, 2619–2633.

70 W. Na, Z. Qu, X. Chen and X. Su, A turn-on fluorescent probe for sensitive detection of sulfide anions and ascorbic acid by using sulfanilic acid and glutathione functionalized graphene quantum dots, *Sens. Actuators, B*, 2018, **256**, 48–54.

